BOLETIN DE LA SOCIEDAD ESPAÑOLA DE
Cerámica y Vidrio
A R T I C U L O

Belite Portland Clinkers. Synthesis and Mineralogical Analysis

A. G. DE LA TORRE,[1*] M. A. G. ARANDA,[1] A. H. DE AZA,[2] P. PENA[2] and S. DE AZA[2]
[1]Departamento de Química Inorgánica, Universidad de Málaga, Teatinos s/n, 29071 Málaga, Spain
[2]Instituto de Cerámica y Vidrio, CSIC, c/ Kelsen nº 5, Campus de Cantoblanco, 28049 Madrid, Spain. *mgd@uma.es

The quaternary system CaO-SiO_2-Al_2O_3-Fe_2O_3 has been taken into account to design five compositions of belite Portland clinkers with belite (Ca_2SiO_4) contents ranging from 60 to 65 wt%, located in its primary phase field of crystallization. The synthesis of these belite clinkers has been studied by high temperature microscopy, dilatometry, differential thermal analysis and thermogravimetric analysis. As a result, the optimum clinkerization temperature has been established at 1360 ± 5ºC. The quantitative phase analyses of the clinkers were carried out by X-ray powder diffraction with the Rietveld methodology. The mineralogical composition depends on the initial dosages, on the highest temperature achieved and on the time of residence at this temperature. The reaction was completed at 1365ºC during 15 min (free CaO <0.5 wt%), in those conditions the β-belite form is stabilized and the harmful transformation β→γ is avoided.

Keywords: Belite Portland clinkers, Phase Equilibrium Diagrams, Rietveld Method

Clínqueres Pórtland Belíticos. Síntesis y Análisis Mineralógico.

Teniendo en cuenta el sistema cuaternario CaO-SiO_2-Al_2O_3-Fe_2O_3, se han diseñado cinco composiciones de clínqueres Pórtland belíticos, con contenidos del 60 y del 65% en peso de belita (Ca_2SiO_4), situadas en su campo primario de cristalización. La síntesis de estos clínqueres belíticos se ha estudiado "in situ" por microscopía de alta temperatura, dilatometría y análisis térmico diferencial y termogravimétrico. La temperatura óptima de clinquerización, determinada con estas técnicas, ha sido de 1360 ± 5ºC. Los análisis cuantitativos de los clínqueres se llevaron a cabo por difracción de rayos-X con la metodología Rietveld. Los porcentajes de las diferentes fases dependen de las dosificaciones iniciales, de la temperatura alcanzada y del tiempo de residencia a dicha temperatura. Se ha conseguido una reacción total (%CaO libre < 0.5% en peso) tratando a 1365ºC durante 15 min, en cuyas condiciones se estabiliza la forma β de la belita y se evita la transformación perjudicial β→γ.

Palabras clave: Clínqueres Pórtland belíticos, diagramas de equilibrio, método de Rietveld.

1. INTRODUCTION

The production of one ton of standard Portland cement releases into the atmosphere 0.54 ton of CO_2 resulting from the decomposition of calcite. In addition, the process uses vast amounts of energy, particularly for clinkering and milling. Thus, to obtain a ton of cement requires to use 60–130 kg of fuel and an average 110 Kwh of power, which result in the release of CO_2 resulting from oxidation of the fuel in the furnace and from the use of fossil fuels to obtain electrical power. The production of Portland cement using coal as fuel releases ~ 0.97 ton of CO_2 per ton of clinker. The overall CO_2 emissions of the cement industry are ~ 6% of all anthropogenic carbon dioxide and account for 4% of the global warming of the planet (1). Finding effective ways of reducing such emissions should therefore be a strong research priority. The production of belite Portland cements is one of such solution as it releases decreased amounts of CO_2.

Standard Portland clinker contains four major crystalline components, namely: alite (Ca_3SiO_5), belite (Ca_2SiO_4), ferrite ($Ca_4Al_2Fe_2O_{10}$) and tricalcium aluminate ($Ca_3Al_2O_6$), in approximate proportions of 60, 15, 10 and 10 wt%, respectively (2). In cement nomenclature, these components are designated C_3S, C_2S, C_4AF and C_3A, respectively, with C = CaO, S = SiO_2, A = Al_2O_3 and F = Fe_2O_3. The formation of the principal component, alite, requires the use of a clinkering temperature of about 1450 ºC in the furnace in the absence of additional melting agents. Conversely, belite Portland clinkers contain more than 50 wt% of belite as the main crystal phase, in addition to alite, ferrite and tricalcium aluminate (3). These clinkers therefore contain less calcium than do standard Portland cements; as a result, their production releases less CO_2 from the decomposition of calcite into the atmosphere (0.50 ton CO_2 per ton of clinker). In addition, the optimum clinkerization temperature for these clinkers is roughly 100 ºC lower than that for standard Portland clinker, which helps to reduce CO_2 emissions from fuel burning.

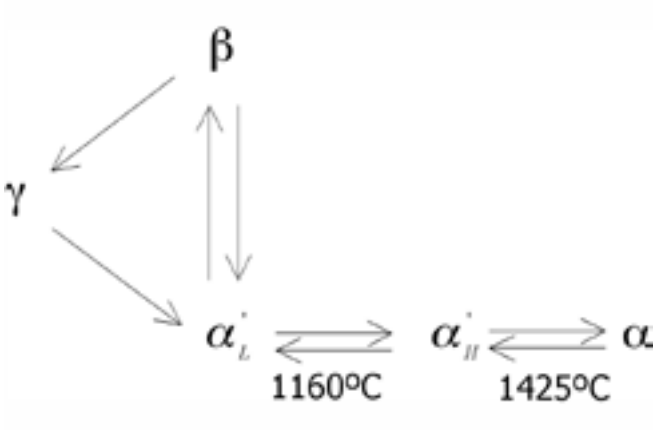

Fig. 1.- Polymorphic transformations of Ca_2SiO_4 with heating (2).

Belite Portland cements provide more durable concretes than does standard Portland cement; however, belite cement is more difficult to mill and reacts more slowly with water. This entails making the belite reactive, whether by stabilizing its high-temperature polymorphs, by decreasing its crystal size or both (5). Stoichiometric C_2S occurs as five different polymorphs (Fig. 1) being the β form which prevails in standard Portland cement; contributing its hydration products to concrete strengthening, particularly after 28 days of curing (2). Belite α forms are more reactive than all others, so they require to be stabilized at room temperature. This can be accomplished by alkalis, sulphur or barium additions or by quenching from 1300 to 900 ºC (6,7). These treatments are intended to offset the low reactivity of β-belite relative to C_3S and hence to obtain a high strength at early curing stages. Some authors have obtained reactive belite phases containing sulphur (8); others have developed alternative production methods involving temperatures below 1350 ºC (e.g. hydrothermal synthesis followed by calcination at a moderate temperature) (9).

On the other hand, a combination of Rietveld methodology (10) and X-ray powder diffraction (XRPD) is the most efficient tool for the quantitative phase analysis (QPA) of mixtures of crystalline substances (11, 12). This approach uses no standard, but requires the prior knowledge of the crystal structures of all the phases present as it involves comparing a theoretical XRD pattern —obtained from the crystal structures— and the experimental one, provided by the diffractometer.

In this work, belite Portland clinkers with five different compositions were prepared based on previously reported

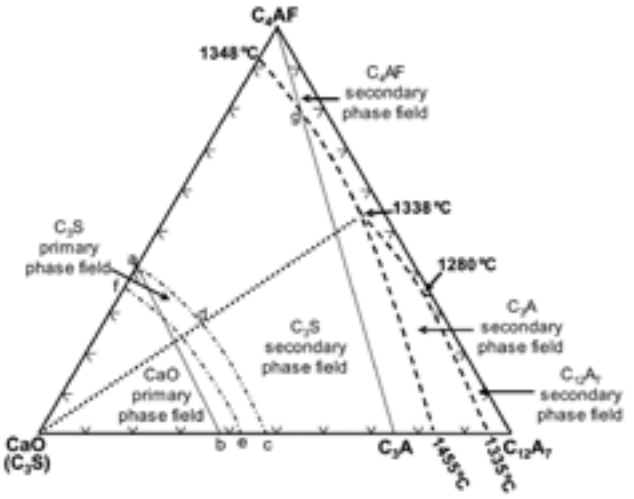

Fig. 2.- Projection of the eutectic surface bounding the primary phase field of crystallization of C_2S for a plane of 65 wt% C_2S onto the opposite side CaO–$C_{12}A_7$–C_4AF of the tetrahedron. The secondary crystallization area for each component and the primary crystallization fields for C_3S and CaO are also shown.

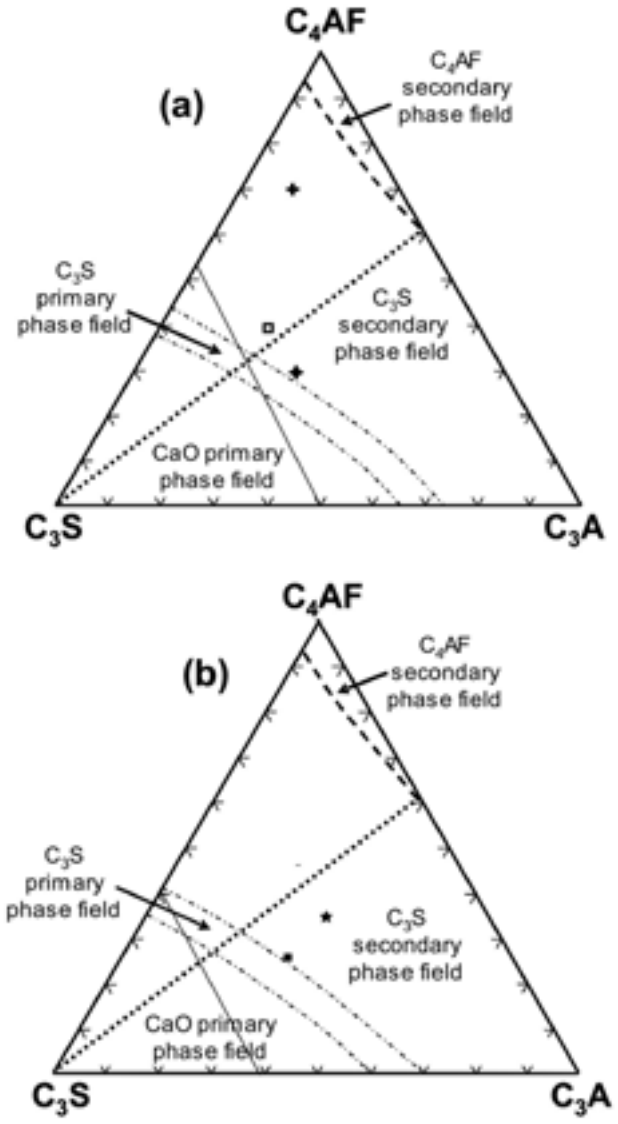

Fig. 3.- Projections of the eutectic surfaces bounding the primary phase field of crystallization of C_2S onto the opposite side C_3S–C_3A–C_4AF of the tetrahedron for the planes: (a) 60 wt% C_2S (the symbols N, ✦ and ~, denote the compositions of B60_1, B60_2 and B60_p, respectively) and (b) 65 wt% C_2S (the symbols "c", "★" and "m", denote the compositions of B65_1, B65_2 and B65_3, respectively). The secondary crystallization area for each component and the primary crystallization fields for C_3S and CaO are also shown.

TABLA I. DOSAGES, AS OXIDE PERCENT WEIGHTS, USED TO OBTAIN THE DIFFERENT BELITE CLINKERS. VALUES OF DIFFERENT PARAMETERS AND THE THEORETICAL MINERALOGICAL COMPOSITIONS OF THE CLINKERS.

Clinker	CaO/%	SiO_2/%	Al_2O_3/%	Fe_2O_3/%	K_2O/%	Na_2O/%	LSF	AR	SR	C_2S/%	C_3S/%	C_4AF/%	C_3A/%
B60_1	63.16	25.12	6.37	5.25	0.08	0.02	78	1.21	2.16	60	16	16	8
B60_2	63.80	25.11	7.04	3.94	0.09	0.02	78	1.79	2.29	60	16	12	12
B65_1	62.70	25.52	6.39	5.28	0.08	0.02	76	1.21	2.19	65	11	16	8
B65_2	63.41	25.59	6.98	3.91	0.09	0.02	77	1.79	2.35	65	11	12	12
B65_3	64.27	26.52	6.13	2.99	0.08	0.02	77	2.05	2.91	65	15	9	11
B60_p	60.31	23.00	7.38	9.19	0.09	0.03	76	0.8	1.39	60	8	28	4

TABLA II. CHEMICAL COMPOSITION OF THE CALCITE AND KAOLIN USED TO OBTAIN THE BELITE CLINKER RAW MIXTURES.

	Calcite	Kaolin
CaO	56.01	0.31
SiO_2		48.59
Al_2O_3		37.13
Fe_2O_3		0.25
K_2O		0.13
Na_2O		0.46
MgO	0.016	0.05
TiO_2		0.01
SrO	0.005	
SO_3	0.011	
LOI (1000 °C)	43.96	13.07

data for the quaternary system CaO–SiO_2–Al_2O_3–Fe_2O_3 (13–15), within the subsystem, C_2S–C_3S–C_3A–C_4AF is comprised. This quaternary phase equilibrium diagram was developed using the projection method (16, 17). The clinkering process was studied in situ by using high-temperature microscopy, dilatometry, differential thermal analysis and thermogravimetry. All phases detected were quantified by using the Rietveld method.

2. EXPERIMENTAL

2.1. Formulation of belite clinkers. Representation and projection methods

Based on the solid state compatibilities of C_2S within the CaO–SiO_2–Al_2O_3–Fe_2O_3 system, and assuming that C_2S would form no solid solution to an appreciable extent, a tentative projection, in the C_2S–$C_{12}A_7$–C_4AF–CaO sub-system, of the binary eutectic surface defining the primary crystallization volume of C_2S on the opposite side $C_{12}A_7$–C_4AF–CaO of the tetrahedron was made, for a plane of 65 wt% of C_2S. The projection is shown in Fig. 2. In all the figure, C_2S is the primary crystallization phase except in the regions designated a-c-e-f and f-e-CaO, where the primary phases are C_3S and CaO, respectively —in fact, their primary crystallization volumes intersect the plane of 65 wt% of C_2S. The bold dashed lines are the projections of the ternary eutectic lines (monovariant lines) defining the secondary crystallization fields of the different phases. The figure also shows the projections of the invariant points for the sub-systems C_2S–$C_{12}A_7$–C_3A–C_4AF (eutectic, 1280 ºC) and C_2S–C_3S–C_3A–C_4AF (peritectic, 1338 ºC). The solid straight lines a–b and C_4AF–C_3A are the intersections of the compatibility triangles C_3S–C_3A–C_4AF and C_2S–C_3A–C_4AF respectively with the plane of 65 wt% C_2S. These lines define the compatibility areas where, in the solid state, the following phases coexist: CaO–C_4AF–C_3S–C_3A (zone CaO-a-b), C_2S–C_3S–C_4AF–C_3A (zone a-b-C_3A–C_4AF) and C_2S–C_3A–C_4AF–$C_{12}A_7$ (zone C_3A-C_4AF–$C_{12}A_7$).

Based on the previous projection, the composition zone for obtaining belite clinkers, containing C_3S as a secondary phase, is restricted to the area bounded by a-c-C_3A-g-1348. The auxiliary dotted line connecting the CaO vertex with the peritectic point at 1338 ºC splits such a zone in two areas. In the upper portion, the phase sequence during crystallization will be: $C_2S + L \rightarrow C_2S + C_3S + L \rightarrow C_2S + C_3S + C_4AF + L \rightarrow C_2S + C_3S + C_4AF + C_3A + L \rightarrow C_2S + C_3S + C_4AF + C_3A$ and in the lower portion it will be: $C_2S + L \rightarrow C_2S + C_3S + L \rightarrow C_2S + C_3S + C_3A + L \rightarrow C_2S + C_3S + C_3A + C_4AF + L \rightarrow C_2S + C_3S + C_3A + C_4AF$ (L denotes "liquid phase").

In order to formulate and represent the composition of the clinkers, as a function of the phases constituting belite clinkers (viz. C_2S, C_3S, C_4AF and C_3A), two additional projections, in the C_2S–C_3S–C_4AF–C_3A sub-system, of the binary eutectic surface defining the primary crystallization volume for C_2S on the opposite side C_3S–C_4AF–C_3A of the tetrahedron were obtained, for the planes corresponding to 60 and 65 wt% C_2S. The projections are shown in Fig. 3. In the figure, the lines and the areas they bound have the same meaning as those in Fig. 2. As can be seen, invariant points fall outside both projections, and so do virtually all eutectic lines. Figure 3a depicts two of the compositions [viz. B60_1 (N) and B60_2 ✦] and Fig. 3b the other three [viz. B65_1 c, B65_2 ★ and B65_3 (■)]. All formulations have been theoretically designed with C_3S proportions greater than 10 wt%, as this phase is very important in ensuring adequate strength at early curing stages.

2.2. Synthesis of belite clinkers

Table I shows the dosages, as oxides, used to prepare each belite clinker. It also shows the theoretical mineralogical composition, lime saturation factor (LSF), alumina ratio (AR) and silica ratio (SR) of each. These parameters are defined as follows:

$$LSF = 100CaO/(2.8SiO_2 + 1.2Al_2O_3 + 0.65Fe_2O_3);$$

$$AR = Al_2O_3/Fe_2O_3;$$

$$SR = SiO_2/(Al_2O_3 + Fe_2O_3)$$

Belite clinker has a low LSF value relative to standard Portland cement (75–80 vs 94–99) (7).

Raw mixtures were prepared by weighing appropriate amounts of the four raw materials: calcite, kaolin, quartz and iron oxide. Calcium was supplied as Merck reagent-grade $CaCO_3$. The source of aluminium, which also contained silicon, was a kaolin from Caobar (Spain), the mineralogical composition of which, as determined by X-ray powder diffraction, was kaolinite [$Al_2Si_2O_5(OH)_4$] plus small amounts of α-quartz (α-SiO_2) and trace of muscovite [$KAl_2(AlSi_3O_{10})(OH)_2$]. The kaolin dosage used was based on the total Al_2O_3 and SiO_2 contents (Table II). The silicon deficiency was corrected by adding α-quartz (99.59% ABCR). Finally, the iron source was Fe_2O_3 (99.95% AlfaAesar). Mixtures were blended by hand in an agate mortar with the aid of ethyl alcohol and dried in a stove at 60 C. This treatment was performed by triplicate.

All raw mixtures were pressed at about 150 MPa into pellets of ~ 1.8 g with ~ 16 mm of diameter. The pellets were placed on Pt/Au crucibles and heated at 5 ºC/min to 900ºC, which was held for 30 min. Then, the temperature was raised at 5 ºC/min up to 1365 ºC and held for 15 min. Finally, the samples were quenched in air at a rate of approximately 2000 ºC/min between 1365 and 800 ºC.

A second set of pellets, with the same composition, was subjected to a slightly different thermal treatment. Thus, the temperature was raised at the same rates, but the holding time at 1365 ºC was 2 h rather than 15 min. The quenching conditions were the same as before. We shall henceforth use "_ b" to designate the raw mixtures treated at 1365 ºC for 2 h (e.g. the B60_1 composition thus processed is named B60_1_b).

2.3. Analytical techniques

The analytical composition of the calcite used (Table II) was determined by X-ray fluorescence spectroscopy on a Phillips PW-1404 spectrophotometer and that of the kaolin (Table II) by inductively coupled plasma atomic emission spectroscopy (ICP-AES) on an IRIS Advantage instrument from Thermo Jarrel Ash.

The thermal behaviour of the raw mixtures was examined by high-temperature microscopy (HTM), using Leica equipment (Wetzlar, Germany) and an alumina support. Samples were heated up to 1525 ºC at a rate of 5 ºC/min. The instrument was equipped with an automatic image analysis system (EMI v. 1.5). The dilatometric profile for each raw mixture was recorded on a Setsys 16/18 dilatometer from Setaram, using a heating rate of 5 ºC/min up to 1320 ºC. Finally, the differential thermal and thermogravimetric analysis (DTA–TG) of the raw mixtures were performed in platinum crucibles, using a Netzsch STA 409 instrument equipped with a TASC 414/2 controller; samples were heated up to 1450 ºC at a rate of 5 ºC/min in an air stream.

X-ray powder diffraction data were obtained at room temperature on a Siemens D5000 diffractometer with θ/2θ geometry (reflection), $CuK_{\alpha 1,2}$ (1.542 Å) radiation and a curved secondary graphite monochromator. Samples were vertically loaded into the methacrylate holder and rotated at 15 rpm during the measuring period. The diffractometer optics comprised three slits of 2 (divergence), 2 (anti-divergence) and 0.2 mm (reception). The X-ray tube was operated at 40 kV at 30 mA. Scans were done with a step size of 0.03º over the 2θ range from 10 to 70º. The step time was 18 s (10 h/ pattern) for the clinkers obtained in 15 min and 5 s (2.8 h/ patterns) for those obtained in 2 h.

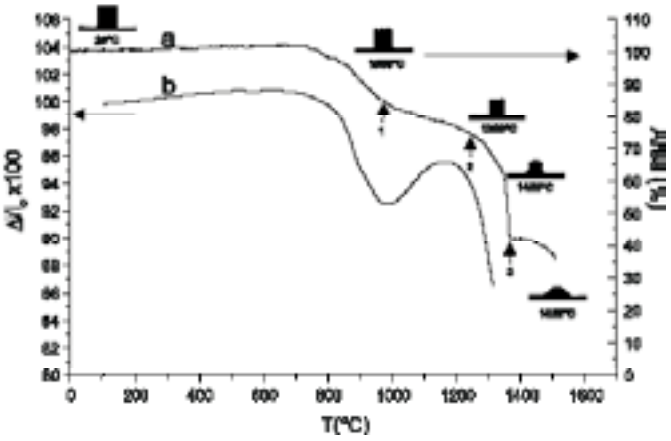

Fig. 4.- (a) Variation of the area as a function of temperature for sample B65_1. (b) Dilatometric curve for the same sample as a function of temperature.

2.4. Analysis of XRPD patterns

X-ray powder diffraction patterns were analysed by using the Rietveld method as implemented in the GSAS software package (18). Peak shapes were determined by using the pseudo-Voigt function (19) with its associated axial divergence correction (20). The Gaussian part of all the phases was fixed, whereas the Lorentzian part of those phases at high proportions was freely refined.

3. RESULTS AND DISCUSSION

The clinkering and melting processes of the raw mixtures were examined by high-temperature microscopy. Samples were pressed into cylindrical pellets 3 mm high × 2 mm in diameter. This size ensured that surface tension forces during

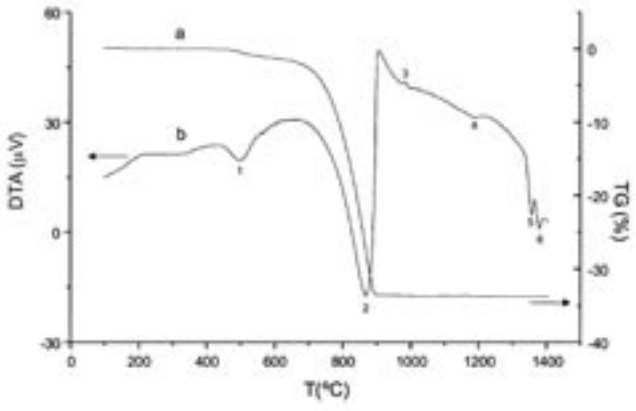

Fig. 5.- (a) Thermogravimetric (TG) and (b) differential thermal analysis (DTA) curves for sample B60_1.

the melting process would be much greater than hydrostatic pressure. The images obtained were used to determine the onset of sintering, its maximum, the softening point and the melting point (half-sphere). As an example, Fig. 4 shows the variation of the area as a function of temperature for sample B65_1 [curve a] as obtained by HTM. The figure also includes selected images illustrating the changes observed. Curve b is the dilatometric profile [i.e. the sintering curve ($\Delta l/l \times 100$)] for the same raw mixture. As can be seen, above ~ 800 ºC the raw mixture started to shrink through decarbonation. This process was subsequently offset by the strong expansion observed between about 1000 and 1180 ºC in the dilatometric profile (Fig. 4, curve b), which resulted in a slope change between about 980 (point 1) and 1250 ºC (point 2) in curve a. This suggests the occurrence of expansive chemical reactions over this temperature range. The combined analysis of the dilatometric and area change data reveals that chemical reactions (e.g. belite formation) prevail over sintering in such a range. At point 2 (~ 1250 ºC in Fig.4, curve a), sintering regains its prevalence by effect of the formation of a liquid phase; as the proportion in such a phase rises, the contraction rate of the raw mixtures substantially increases between points 2 (1250 ºC) and 3 (1358 ºC). The above-described behaviour was virtually identical for the five mixtures studied.

Fig. 5 shows the DTA and TG curves for mixture B60_1, as a representative example for all the compositions. Curve a shows mass changes as a function of temperature (TG). Curve b is the differential thermal analysis (DTA) profile. A small endothermic peak, corresponding to a weight loss resulting from the dehydroxylation of kaolin, is observed at ~ 500 ºC (point 1). The endothermic peak at ~ 880 ºC (point 2), with a substantial weight loss associated, is due to the decomposition of $CaCO_3$. The sharp exothermic peak at ~ 980 ºC (point 3) corresponds to the coordination change of aluminium in meta-kaolin (amorphous) during its transformation into a spinel-like transient phase prior to the formation of mullite (21, 22). An additional, very small endothermic peak is observed at ~ 1190 ºC (point 4), which coincides with the invariant point for the mullite–silica–feldspar sub-system (23) and can be assigned to the formation of a transient liquid due to impurities present in the kaolin. Finally, the curve includes two endothermic peaks at high temperatures. One, at ~ 1350 ºC (point 5) for the five raw mixtures, corresponds to the formation of a permanent liquid phase. The other, at ~ 1380 ºC (point 6), corresponds to the $\alpha'_H \rightarrow \alpha$ transformation in belite upon heating (24).

From the area changes, dilatometry, DTA and TG data, the optimum clinkerization temperature for all the compositions

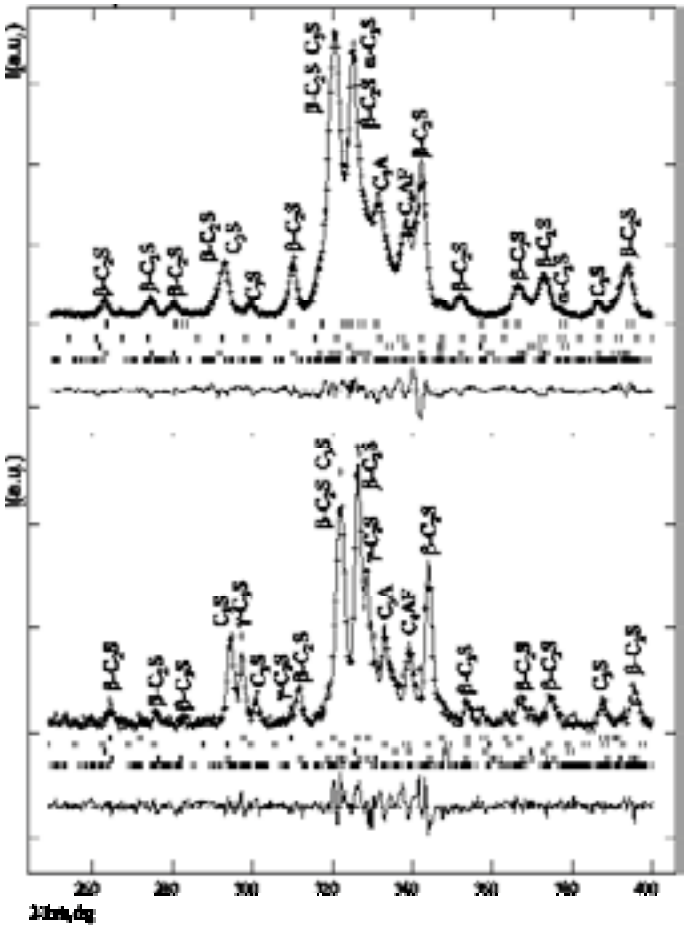

Fig. 6.- Selected range of the Rietveld plots for clinker B65_1 (top) and B65_1_b (bottom). The major peaks for each phase are labelled.

was established to be at 1360 ± 5 ºC. The raw mixtures were therefore thermally treated at 1365 ºC for 15 min, as previously described, in order to obtain the corresponding clinkers. The QPA for the clinkers were determined by using the Rietveld method; the results are shown in Table III together with the agreement factors (weight profile R-factor) for each refinement. The table also gives the references to the structural descriptions used to obtain the theoretical XRPD patterns for each phase. The Rietveld results are normalized to 100% crystallinity (i.e. the presence of amorphous, non-diffracting phases was excluded). All samples were found to contain

TABLA III. RESULTS OF RIETVELD QPA OF BELITE CLINKERS OBTAINED BY HEATING AT 1365 ºC/15 MIN. THE DATA ARE NORMALIZED TO 100% CRYSTALLINITY. THE AGGREMENT FACTOR (R_{WP}) FOR EACH FIT IS ALSO SHOWN.

Clinker	β-C_2S %	α-C_2S %	total C_2S /%	C_3S %	C_4AF %	C_3A %	R_{WP} %
B60_1	54.8(2)	2.6(3)	57.4	20.1(3)	13.3(2)	9.2(2)	9.4
B60_2	52.1(3)	3.4(4)	55.5	21.6(3)	8.1(2)	14.8(2)	10.5
B65_1	63.0(2)	4.3(5)	67.3	11.8(3)	12.4(2)	8.5(2)	9.7
B65_2	60.6(2)	2.0(3)	62.6	14.6(3)	8.0(2)	14.8(2)	9.9
B65_3	61.3(2)	-	61.3	18.0(3)	5.3(2)	15.4(2)	9.7
Reference/ Structure	(25)	(25)		(26)	(27)	(28)	

TABLA IV. RESULTS OF RIETVELD QPA OF BELITE CLINKERS OBTAINED BY HEATING AT 1365 ºC/2 H. THE DATA ARE NORMALIZED TO 100% CRYSTALLINITY.

Clinker	β-C_2S/%	γ-C_2S/%	Total C_2S /%	C_3S/%	C_4AF/%	C_3A/%
B60_1_b	46(1)	6(1)	52	33(1)	7(1)	8(1)
B60_2_b	46(1)	5(1)	51	30(1)	6(1)	13(1)
B65_1_b	45(1)	15(1)	60	25(1)	9(1)	6(1)
B65_2_b	49(1)	9(1)	58	25(1)	6(1)	11(1)
B65_3_b	51(1)	8(1)	59	25(1)	4(1)	12(1)

β-C_2S, C_3S, C_4AF and C_3A. Free CaO was never present in amounts greater than 0.3 wt%; consequently, the degree of clinkerization under these conditions was quite adequate. Four clinkers contained a small amount of α'_H-C_2S (see Table III). Heating for only 15 min at 1365 ºC, followed by quenching in air, ensured the absence of the β-C_2S → γ-C_2S transformation in all cases. This polymorphic transformation during cooling must be avoided since γ form is hydraulically inactive.

As an example, Fig. 6 shows a selected portion of the Rietveld plots for the clinkers B65_1 and B65_1_b. The peaks mainly due to a given phase are labelled. The lower curve, in each pattern, represents the difference between the theoretical and experimental data; the flatter it is, the higher is the quality of the analysis.

The mineralogical composition obtained (Table III) is very similar to the theoretical composition calculated from the solid state compatibilities (Table I). The proportion of C_3S always exceeded 10 wt%, which is highly desirable for the above-described reasons. However, it also highly desirable to stabilize an increased amount of the α-C_2S in order to activate the cements and to obtain a higher strength at early stages during the curing process. Studies on these subjects are currently under way.

Additionally, an interesting result which brings information about the location of the invariant point of the C_2S–C_3S–C_3A–C_4AF system has to be pointed out. Thus, the proportion of the ferrite phase, C_4AF, was always below its theoretical value and its diffraction peaks were very broad. To clarify this, the full width at the half maximum (FWHM) of the 2θ ~ 12º peak for C_4AF in clinker B60_1 was measured, being 0.24º. This value suggests that the C_4AF phase crystallizes during cooling, consequently the auxiliary line connecting the CaO vertex with the invariant point (Figs 2 and 3) should lie above all the selected compositions rather than as tentatively shown in Figs 2 and 3. In order to fork the location of the invariant point, a new composition in the 60 wt% C_2S plane was prepared, namely B60_p, **+**, (see Fig. 3a and Table I). This raw mixture was subjected to the thermal treatment for the b series and the FWHM for the same C_4AF diffraction peak was measured and found to be 0.09º. This lower value indicates that the C_4AF diffraction domains in this clinker are larger than in clinker B60_1 (i.e. that it had enough time to crystallize and grow). In addition, in clinker B60_p it was the C_3A phase that showed the broadest peaks. Consequently, the auxiliary dotted line should lie in between those for B60_1 and B60_p.

The influence of the clinkering time on the growth of belite crystals was examined by heating the previous compositions at the same temperature but a longer time (2 h). Obviously, the belite crystals in the new clinkers should be larger. This is being currently studied by electron microscopy. However, the results so far confirm that quenching in air fails to completely prevent the β-C_2S → γ-C_2S transformation in this samples (see Fig. 6, bottom). The QPA for these clinkers are shown in Table IV. As can be seen, there was no trace of the most reactive phase of belite (α'_H-C_2S), however, there was an appreciable amount of the non-hydraulic form (γ-C_2S). On the other hand, a longer period of heating at 1365 ºC yields to higher proportions of alite in these compositions (Table IV). Consequently, belite Portland clinkers should be clinkered for a short time at 1365 ºC in order to avoid substantial growth of belite crystals which prevent the harmful transformation of β → γ during cooling.

4. CONCLUSIONS

The projection of the eutectic surface bounding the primary field of crystallization of C_2S in the C_2S–C_3S–C_3A–C_4AF system allowed locating within such a volume two series of belite clinkers with 60 and 65 wt% C_2S, respectively, and variable proportions of C_3S, C_3A and C_4AF.

HTM, DTA, TG and dilatometric studies allowed establishing 1365 ± 5 ºC as the optimum clinkerization temperature. Thermal treatment of the raw mixtures at such temperature for 15 min allowed to obtain clinkers with β-C_2S —containing a small amount of α form— and to avoid the harmful transformation β → γ. However, such transformation could not be avoided with increasing time of treatment.

The Rietveld method to obtain QPA was extended to belite Portland clinkers.

REFERENCES

1. R. McMacffrey. «Climate change and the cement industry». Global Cement and lime magazine; Environmental Special Issue 2002.
2. H.F.W. Taylor. «Cement Chemistry», 2nd ed. Thomas Telford Ltd (London) 1997.
3. J. Bensted, P. Barnes. «Structure and Performance of Cements», 2nd ed. Spon Press (London) 2002.
4. U. Ludwig, R. Pohlmann. «Investigations on the production of low lime portland cements». Sub Theme 1.3 Vol. **II**, 363–371, Eighth International Congress on the Chemistry of Cement (8th ICCC), Rio de Janeiro (Brasil), 1986.
5. A.K. Chatterjee. «High belite cements—Present status and future technological options: part I». Cement and concrete research **26**[8] 1213–1225 (1996).
6. A. Gies, D. Knofel. «Influence of alkalies on the composition of belite-rich cement clinkers and the technological properties of the resulting cements». Cement and Concrete Research **16**[3] 411–422 (1986).
7. A.K. Chatterjee. «High-belite Portland cement. An update on development, characterization and applications», pp 31–40 in Proceedings of the 11th International Congress on the Chemistry of Cement (ICCC), Durban (South Africa), May 2003.
8. C.D. Popescu, M. Muntean, J.H. Sharp. «Industrial trial production of low energy belite cement». Cement and Concrete Composites **25** 689–693 (2003).
9. A. Guerrero, S. Goñi, I. Campillo, A. Moragues. «Belite cement clinker from coal fly ash of high Ca content. Optimization of synthesis parameters».

Environ. Sci. Technol. **38** 3209–3213 (2004).
10. H.M. Rietveld. «A profile refinement method for nuclear and magnetic structures». J. Appl. Crystallogr. **2** 65–71 (1969).
11. I.C. Madsen, N.V.Y. Scarlett, L.M.D. Cranswick, T. Lwin. «Outcomes of the International Union of Crystallography Commission on powder diffraction round robin on quantitative phase analysis: samples 1a to 1h». J. Appl. Crystallogr. **34** 409–426 (2001).
12. N.V.Y. Scarlett, I.C. Madsen, L.M.D. Cranswick, T. Lwin, E. Groleau, G. Stepheson, M. Aylmore, N. Agron-Olshina, «Outcomes of the International Union of Crystallography Commission on powder diffraction round robin on quantitative phase analysis: samples 2, 3, 4, synthetic bauxite, natural granodiorite and pharmaceuticals». J. Appl. Cryst. **35**, 383–400 (2002).
13. F.M. Lea, T.W. Parker. «Investigation on a portion of the quaternary system $CaO–Al_2O_3–SiO_2–Fe_2O_3$». Trans. Roy. Soc. (London), **234A** 1–42 (1934).
14. J. W. Greig. Am. J. Sci. **13** 1–44 (1927).
15. M.A. Swayze, «A report on studies of :1. The ternary system $CaO–C_5A_3–C_2F$ .2.The quaternary system $CaO–C_5A_3–C_2F–C_2S$ .3. The quaternary system as modified by 5-percent magnesia». Am. J. Sci. **244**[1] 1–30 (1946)
16. P. Pena, B. Vázquez, A. Caballero, S. de Aza. «Diagramas de equilibrio de fases cuaternarios. Método de interpretación y representación». Bol. Soc. Esp. Ceram. V., **44**[2] 113-122 (2005).
17. P. Pena, S. de Aza. «Metodología para el estudio de diagramas de equilibrio cuaternarios. Aplicación al sistema $ZrO_2–Al_2O_3–SiO_2–TiO_2$». Jornadas Científicas sobre Cerámica y Vidrio, University of Barcelona, pp 255–297 (1980).
18. A.C Larson,. R.B. Von Dreele. «General Structural Analysis System». Los Alamos National Lab. Rep. No. LA-UR-86-748. GSAS program @ http://public.lanl.gov:80/gsas/, 1994.
19. P. Thompson, D.E. Cox, J.B. Hasting. «Rietveld refinement of Debye–Scherrer synchrotron X-ray data from Al_2O_3». J. Appl. Crystallogr. **20** 79–83 (1987).
20. L.W. Finger, D.E. Cox, A.P. Jephcoat. «A correction for powder diffraction peak asymmetry due to diaxial divergence». J. Appl. Crystallogr. **27** 892–900 (1994).
21. J. Sanz, A. Madani, J. M. Serratosa, J. S. Moya, S. De Aza. «Aluminium-27 and silicon-29 magic-angle spining nuclear magnetic resonance study of the kaolinite–mullite transformation». J. Am. Ceram. Soc., **71[10]** C-418–C-421 (1988).
22. J. Sanz, I. Sobrados, A. L. Cavalieri, P. Pena, S. De Aza, J. S. Moya. «Structural changes induced on mullite precursors by thermal treatment: A ^{27}Al MAS-NMR investigation». J. Am. Ceram. Soc., **74[10]** 2398–403 (1991).
23. J. Espinosa de los Monteros, S. De Aza, M. A. del Rio, E. Criado. «Aplicación de los diagramas de fases ternarios a los productos de cerámica blanca». Bol. Soc. Esp. Ceram. V., **12**[1] 31–39 (1973).
24. K. Fukuda, A. Takeda, H. Yoshida. «Remelting reaction of α-Ca_2SiO_4 solid solutions confirmed in $Ca_2SiO_4–Ca_{12}Al_{14}O_{33}$ pseudobinary system». J. Am. Ceram. Soc. **31** 1185–1189 (2001).
25. W. G. Mumme, R. J. Hill, G. Bushnell-Wye, E. R. Segnit. «Rietveld structure refinement, crystal chemistry and calculated powder diffraction data for the polymorphs of dicalcium silicate and related phases». N. Jb. Miner. Abh. **169** 35–68 (1995).
26. A.G. De la Torre, S. Bruque, J. Campo, M.A.G. Aranda. «The superstructure of C_3S from synchrotron and neutron powder diffraction and its role in quantitative phase analyses». Cem. Concr. Res. **32** 1347–1356 (2002).
27. A.A. Colville, S. Géller. «The crystal structure of brownmillerite, Ca_2FeAlO_5» Acta Cryst. **B27** 2311–2315 (1971).
28. P. Mondal, J.W. Jeffery. «The crystal structure of tricalcium aluminate, $Ca_3Al_2O_6$». Acta Cryst. B31 689–697 (1975).

Recibido: 14.02.05
Aceptado: 30.03.05